^{177}Lu-Labeled Amidoxime-Functionalized Biodegradable Microspheres for Transarterial Radioembolization of Hepatocellular Carcinoma*

Xingliang Liu†,[1] Gang Wang†,[2] Zhenwen Zhao†,[2] Haoyu Wang,[1] Hongyu Chen,[1] Xiao Xu∗,[3, †] Jingdong Li∗,[1, ‡] and Hongjuan Ma∗[2, §]

[1]Institute of Hepato-Biliary-Pancreatic-Intestinal Disease, Affiliated Hospital of North Sichuan Medical College, North Sichuan Medical College, Nanchong 637100, P. R. China.

[2]Shanghai Applied Radiation Institute, School of Environmental and Chemical Engineering, Shanghai University, Shanghai 200444, P. R. China.

[3]Cancer Center, Guangdong Engineering Research Center of Boron Neutron Therapy and Application in Malignant Tumors, The Tenth Affiliated Hospital, Southern Medical University (Dongguan People's Hospital), Dongguan 523059, P. R. China.

Abstract: Transarterial radioembolization (TARE) has become an important locoregional therapy for hepatocellular carcinoma (HCC). However, the clinically used yttrium-90 (^{90}Y) microspheres are non-biodegradable and provide limited imaging capability, while biodegradable polymeric microspheres prepared through conventional radiolabeling strategies often exhibit poor radionuclide stability. Here, we report a biodegradable radiometal-chelating microsphere based on amidoxime-functionalized polylactic acid microspheres (PLA-g-PAO-Ms) engineered via electron-beam-induced graft polymerization. The resulting PLA-g-PAO-Ms exhibit a high Lu^{3+} loading capacity (33.83 mg g^{-1}) and undergo controlled biodegradation in vitro after approximately 20 days. In a rat orthotopic live tumor model, intra-arterial administration of ^{177}Lu-labeled PLA-g-PAO-Ms (^{177}Lu-PLA-g-PAO-Ms) resulted in pronounced tumor suppression with sustained in vivo radionuclide retention for at least 14 days. Notably, the radiometal chelation strategy enables tunable specific radioactivity of the microspheres through modulation of coordination conditions, offering precise control over therapeutic dose deposition. These findings suggest that PLA-g-PAO-Ms provide a biodegradable microsphere system capable of stable radiometal incorporation and effective tumor suppression following intra-arterial administration, offering a promising approach for interventional radionuclide therapy of HCC.

Keywords: Transarterial radioembolization, Radiation-induced graft polymerization, Biodegradable microspheres, Radiometal chelation, Hepatocellular carcinoma[1]

∗ † These authors contributed equally to this work and act as co-first authors. Supported by the National Natural Science Foundation of China (Grant No. 82502440 and 12475346), Guangdong Basic and Applied Basic Research Foundation Special Projects (Regional Cultivation Project) (Grant No. 2023A1515140032), Innovation Development Fund of China Seawater Uranium Extraction Technology Innovation Alliance (Grant No. CNNC-CXLM-202202 and CNNC-HSTY-2024-004), Sichuan MedicalScience and Technology Innovation Research Association (Grant No. YCH-KY-YCZD2024-026) and Research Projects of Nanchong Municipal Science and Technology Bureau (Grant No. 23JCYJPT0038)

† Corresponding author, xiaoxu721@smu.edu.cn

‡ Corresponding author, lijingdong358@126.com

§ Corresponding author, hongjuanma@shu.edu.cn

1 INTRODUCTION

Hepatocellular carcinoma (HCC) remains a major cause of cancer-related mortality worldwide.[1–3] Radical hepatectomy remains the primary curative treatment for HCC and offers the best chance for long-term survival[4]. For unresectable HCC, clinical management relies on alternative therapeutic strategies, including local ablation, transarterial therapies, external beam radiotherapy (EBRT), and systemic anticancer treatments, with the aim of improving survival and disease control.[5]

TARE is an interventional form of internal radiotherapy that has been widely applied in the treatment of hepatic malignancies. TARE provides localized radionuclide retention within the tumor and enables continuous internal irradiation while largely sparing surrounding normal tissues[6]. In addition, owing to the relatively long tissue penetration range of β radiation, TARE can effectively deliver cytotoxic radiation to tumor cells located deep within the lesion, which may provide advantages over transarterial chemoembolization (TACE) in certain hypovascular tumors[7]. Several key challenges remain in the development of TARE microsphere systems. These include efficient radionuclide loading, stable retention of the radionuclide within tumor tissue, and physicochemical properties that ensure stable suspension and smooth delivery through microcatheters. These parameters critically influence radiation dose distribution and therapeutic efficacy. The ideal microsphere platform should also possess controllable biodegradability. Permanent retention of non-degradable microspheres within the hepatic vasculature may lead to long-term complications such as vascular stenosis or chronic inflammatory responses. Controlled degradation after completion of radionuclide decay could facilitate microsphere clearance from liver tissue, potentially alleviating local hypoxia and reducing hypoxia-driven tumor aggressiveness, while theoretically enabling safer retreatment with subsequent cycles of radioembolization. However, despite increasing research interest in biodegradable radioembolization platforms, no clinically approved microsphere products with predictable and controllable degradation profiles are currently available. Achieving an optimal balance between degradability, radionuclide retention, and therapeutic safety therefore remains a major challenge in the development of next-generation TARE microspheres.[8]

Polylactic acid (PLA) microspheres are widely considered promising carriers for biodegradable radioembolization because of their favorable biocompatibility and tunable degradation properties.[9] However, radiolabeling strategies for PLA-based microspheres often suffer from limited labeling stability and radionuclide leakage *in vitro* and *in vivo*, which has hindered their clinical translation for TARE[10]. Holmium-166 (^{166}Ho)-labeled PLA microspheres represent one of the earliest biodegradable radioactive microsphere systems investigated for TARE. These microspheres are typically produced by encapsulating non-radioactive holmium acetylacetonate ($Ho(acac)_3$) within poly(L-lactic acid) (PLLA) microspheres through an emulsion–solvent evaporation process, followed by neutron activation to convert ^{165}Ho into ^{166}Ho.[11, 12] The high-energy neutron irradiation required for activation can induce radiolytic degradation of the PLA matrix, leading to polymer chain scission and loss of structural integrity. Such damage to the carrier material increases the risk of radionuclide leakage and unintended systemic radiation exposure.[13]

The physical characteristics of currently used radionuclides also impose important limitations on TARE. ^{90}Y, the clinical standard for radioembolization, is a pure β^- emitter that lacks γ-emission suitable for nuclear imaging, preventing direct visualization of microsphere distribution and accurate *in vivo* dosimetry using SPECT. ^{166}Ho emits both β^- particles and γ-rays but has a short physical half-life of 26.8 h, which restricts the duration of intratumoral irradiation and complicates clinical logistics. Lutetium-177 (^{177}Lu) provides several advantages for interventional radionuclide therapy. With a physical half-life of 6.7 days, it allows sustained radiation delivery while maintaining practical flexibility for radiopharmaceutical preparation and administration. Its β^- particles (Emax = 0.497 MeV) have a tissue penetration range of approximately 2 mm, enabling localized tumor irradiation with reduced exposure to surrounding liver tissue. In addition, the concomitant emission of 208 keV γ-rays permits real-time nuclear imaging and quantitative dosimetry using SPECT/CT, supporting image-guided therapy and treatment monitoring. To overcome the limitations associated with conventional radiolabeling strategies, we developed a surface chelation–mediated labeling approach based on amidoxime-functionalized PLA microspheres. Amidoxime (AO) groups were introduced onto the microsphere surface to enable stable coordination with Lu^{3+} ions while preserving the structural integrity of the polymer matrix. Compared with neutron activation–based methods, this strategy enables efficient radiolabeling under mild conditions without radiation-induced damage to the carrier material. The AO ligand exhibits strong affinity for trivalent metal ions and forms stable coordination complexes with Lu^{3+}. Our previous density functional theory (DFT) studies demonstrated that AO groups can generate thermodynamically stable hexadentate chelation structures with favorable enthalpy and Gibbs free energy characteristics.[14, 15] Unlike conventional chelators such as DOTA or EDTA, AO-mediated coordination can be achieved under mild conditions at room temperature, avoiding thermal damage to the microsphere matrix.[16]

In this work, monodisperse PLA microspheres were fabricated using microfluidic technology. Acrylonitrile groups were introduced via electron beam–induced graft polymerization and subsequently converted to amidoxime groups through amidoximation, yielding PLA-g-PAO-Ms. Physicochemical characterization confirmed successful surface functionalization and high ^{177}Lu chelation capacity. The resulting ^{177}Lu-PLA-g-PAO-Ms demonstrated favorable biocompatibility, stable radionuclide retention, and pronounced antitumor efficacy in hepatocellular carcinoma models (Fig. 1). The γ-emission of ^{177}Lu further enabled non-invasive SPECT imaging of microsphere distribution *in vivo*, providing intrinsic theranostic capability.

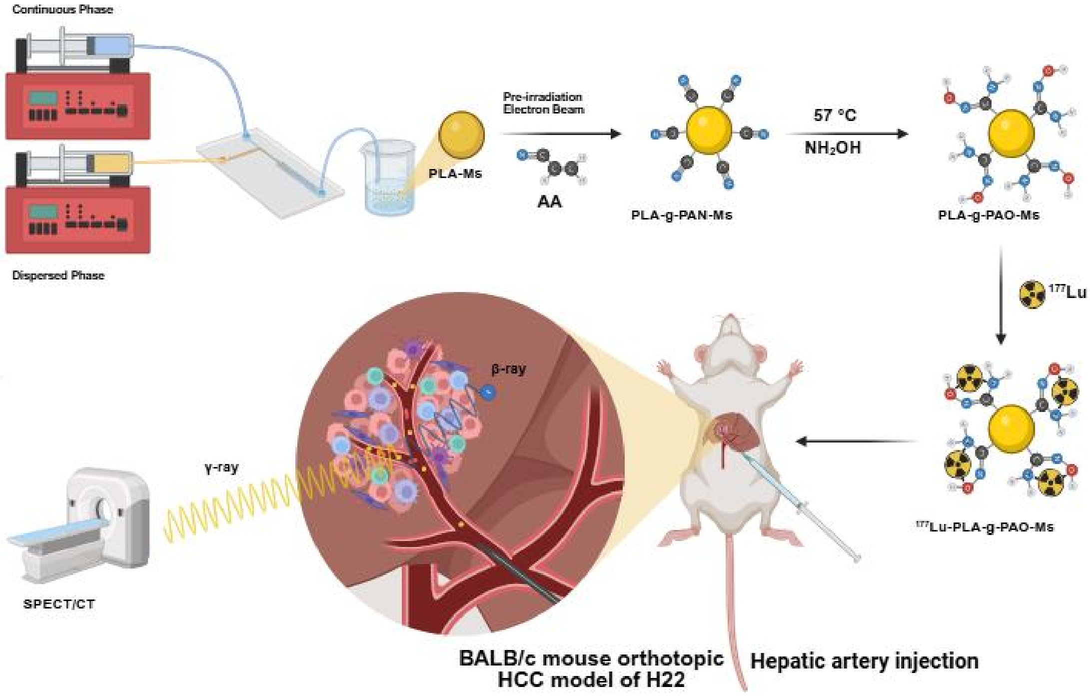

Fig. 1 Schematic illustration of the synthesis and anti-tumor application of PLA-g-PAO-Ms. Monodisperse poly microspheres (PLA-Ms) were first generated by via microfluidic technology. Acrylonitrile monomers was then grafted onto the PLA-Ms surface through electron beam-induced graft polymerization, followed by amidoximation reaction to transform the cyano groups in the grafted chains into amidoxime chelating ligands, thus obtaining the target PLA-g-PAO-Ms. The scheme also outlines the workflow of *in vivo* administration and anti-tumor therapeutic efficacy evaluation of ^{177}Lu-radiolabeled PLA-g-PAO-Ms in a rat orthotopic HCC model. Created in https://BioRender.com

2 MATERIALS AND METHODS

2.1 Materials

PLA (Aladdin, ≥99%), Acetone (Aladdin, ≥99%), methanol (Aladdin, ≥99%), and N,N-dimethylformamide (DMF, Aladdin, ≥99%), Polyvinyl alcohol (PVA, Macklin, ≥99%), Acrylonitrile (AN, Aladdin, ≥99%), Hydroxylamine hydrochloride ($NH_2OH \cdot HCl$, Macklin, ≥99%) and sodium hydroxide (NaOH, Macklin, ≥99%) were used as received. ^{177}Lu chloride ($^{177}LuCl_3$) solution (37 MBq) was used as received. Ultrapure water was used in all experiments.

2.2 Synthesis of PLA-g-PAO-Ms

Preparation of PLA Microspheres (PLA-Ms): PLA-Ms were fabricated via microfluidic technology combined with a phase separation method, which enabled the production of PLA-Ms with uniform diameter, regular morphology, and excellent size controllability by tuning the flow rates of the continuous/mobile phases and solution concentration. To prepare the continuous phase, 1 mL of PLA/acetone solution (15 mg mL^{-1}) was mixed with 1.32 mL of methanol, followed by vortex mixing for 10 min. Meanwhile, 10 mL of 0.25% (w/v) PVA aqueous solution was prepared as the mobile phase. The as-prepared continuous phase and mobile phase were loaded into syringes respectively, and the flow rate ratio of the two phases was precisely adjusted via the syringe plunger to generate uniformly sized dispersed microspheres suspended in the PVA solution. The resulting PLA-Ms were collected by filtration, and the filtrate was freeze-dried and stored for subsequent characterization and further modification.

Preparation of PLA-g-PAO-Ms: Prior to graft polymerization, PLA-Ms were pre-irradiated in nitrogen at room temperature using an electron beam accelerator (Pioneer Electric Company GJ-2-II, Institute of Applied Radiation, Shanghai University), with a beam energy of 2 MeV, a maximum beam current of 10 mA, and a total irradiation dose of 20 kGy. In the graft polymerization reaction, a monomer solution consisting of 3 mL of AN, 1 mL of AA, and 6 mL of DMF was added to a flask, and deoxygenated for 10 min via nitrogen purging. The pre-irradiated PLA-Ms were subsequently added to the flask, and the graft polymerization reaction was carried out at 57°C for 4 h. Upon completion of the reaction, the resulting grafted product was washed with DMF thoroughly to remove residual monomers and homopolymers. After vacuum freeze-drying, the desired product acrylonitrile-functionalized polylactic acid microspheres (PLA-g-PAN-Ms) was successfully prepared. For the amidoximation reaction, 10 g of $NH_2OH \cdot HCl$ was dissolved in 100 mL of ultrapure water, and the pH of the solution was adjusted to neutral with 5.7 g of NaOH. The as-prepared PLA-g-PAN-Ms were dispersed in the neutral $NH_2OH \cdot HCl$ solution, and the mixture was heated to 60 ° C for 12 h to fully convert the cyano groups into AO functional groups. After the amidoximation reaction was completed, the product was centrifuged at 8000 r min^{-1}, the supernatant was discarded, and the solid was washed repeatedly with ultrapure water to remove residual $NH_2OH \cdot HCl$ and NaOH. The final product PLA-g-PAO-Ms was obtained after vacuum drying for 24 h followed by freeze-drying. The chemical structure, microstructure, mechanical properties, functional group density and distribution of the obtained materials were characterized correspondingly.

Radiolabeling of PLA-g-PAO-Ms with ^{177}Lu: 1 mL of PLA-g-PAO-Ms dispersion (30 mg mL^{-1}) was mixed with 10 μL of $^{177}LuCl_3$ solution (37 MBq), and 10 μL of 0.04 M NaOH solution was added to adjust the pH of the mixture to 6–7. The mixture was oscillated at 60°C for 30 min, followed by repeated washing and centrifugation to remove unbound ^{177}Lu.

2.3 Characterization

Fourier-transform infrared (FT-IR) spectra were recorded on a Fourier-transform infrared spectrometer (Bruker GmbH, Germany) with the KBr pellet method to confirm the chemical structure of PLA-g-PAO-Ms, with a scan range of 4000–500 cm^{-1}, a resolution of 4 cm^{-1} and 32 scans per sample.

X-ray photoelectron spectroscopy (XPS) spectra were collected on an X-ray photoelectron spectrometer (Kratos Ltd., UK) with a monochromatic Al Kα X-ray source. Twenty milligrams of PLA-Ms, PLA-g-PAN-Ms, PLA-g-PAO-Ms, and Lu-PLA-g-PAO-Ms were used for the measurements, with the test voltage set to 10 kV, a full-spectrum energy range of 160 eV and a scanning range of 0–1200 eV. The pressure of the analysis chamber was maintained at 1×10^{-9} Torr during the test, and the obtained XPS data were analyzed using Thermo Avantage software.

X-ray diffraction (XRD) patterns were recorded on an X-ray diffractometer (Rigaku Corporation, Japan) with Cu Kα radiation as the excitation source, a scanning range of 5–80° and a scanning rate of 5° min^{-1} to characterize the crystalline structure of PLA-Ms, PLA-g-PAN-Ms, and PLA-g-PAO-Ms.

Scanning electron microscopy (SEM) images were acquired on a field emission scanning electron microscope (JEOL Ltd., Japan) to study the morphological characteristics of PLA-Ms, PLA-g-PAN-Ms, and PLA-g-PAO-Ms. Prior to testing, the microspheres were dried in a vacuum drying oven at 50°C for 6 h, then mounted on sample stubs with double-sided conductive tape and subjected to gold sputtering at a current of 20 mA for 180 s. The morphological observations were conducted at an accelerating voltage of 5 kV.

Contact angles were measured on a contact angle meter (KSV Instruments Ltd., Finland) for PLA-Ms and PLA-g-PAO-Ms pellets, which were prepared by tableting under 5 MPa pressure for 30 s. A 50 μL drop of ultrapure water (18.2 MΩ cm) was dispensed onto the sample surface, with video recording to capture images every 50 ms. Contact angles were determined from the images captured at the moment of droplet-sample contact, and measurements were repeated five times at different positions for each sample.

Thermogravimetric analysis (TGA/DTG) was performed on a TA Instruments Discovery Series TGA 550 Thermogravimetric Analyzer (TA, USA) for PLA-Ms, PLA-g-PAN-Ms, and PLA-g-PAO-Ms under a high-purity nitrogen atmosphere with a flow rate of 50 mL min^{-1}. The measurements were carried out over a temperature range of 25–800°C at a heating rate of 10°C min^{-1}, the temperature corresponding to the maximum thermal degradation rate (T_{max}) of each material was determined from the DTG curves, and the thermal stability of materials during modification was analyzed by comparing the TGA/DTG curves of PLA-Ms, PLA-g-PAN-Ms and PLA-g-PAO-Ms.

Laser diffraction particle size distribution was determined on a Mastersizer 3000 (Malvern Panalytical Ltd., UK) for PLA-g-PAO-Ms in wet dispersion mode with ultrapure water as the dispersant. The samples were ultrasonicated for 5 min before testing for uniform dispersion, the median particle diameter (D50) and the proportion of particles in specific diameter ranges were obtained, and the uniformity of microsphere size distribution was evaluated from the test results.

Dynamic light scattering (DLS) measurements were conducted on a Brookhaven NanoBrook Omni Nanoparticle Size and Zeta Potential Analyzer (Brookhaven, USA) at a scattering angle of 90° to determine the hydrodynamic diameter of PLA-g-PAO-Ms under simulated physiological conditions. A 5 mL suspension of PLA-g-PAO-Ms (10 mg mL^{-1}) was dispersed in phosphate-buffered saline (PBS, pH 7.4, 0.01 mol L^{-1}) and transferred to sterilized centrifuge tubes, which were incubated in a shaking incubator at 37°C with agitation at 200 rpm for 35 days. An aliquot of the suspension was collected every 5 days, and the particle diameter was analyzed immediately; the average particle size was plotted against degradation time to assess microsphere stability and degradation rate.

Inductively coupled plasma mass spectrometry (ICP-MS) measurements were performed on an Thermo Scientific iCAP TQ ICP-MS (Thermo Scientific, USA) to determine the Lu^{3+} concentration in the supernatant of chelation reaction mixtures, with three parallel replicates for each sample and all centrifugation steps conducted at 8000 rpm for 5 min. For pH regulation experiments, a 100 mL Lu^{3+} aqueous solution (1 mg L^{-1}) was prepared and its pH adjusted to 5–9, 0.2 mg of PLA-g-PAO-Ms was added and incubated at 37 °C with shaking at 150 rpm, and 1 mL of supernatant was collected at 10, 20, 30, and 60 min then transferred to 2% (v/v) HNO3 for analysis. For different initial concentration experiments, 100 mL Lu^{3+} solutions (0.1, 1, 10 mg L^{-1}) with pH adjusted to 7 were used with the same chelation and testing procedure. For different solid-liquid ratio experiments, 0.1, 0.2, and 2 mg of PLA-g-PAO-Ms were added to 100 mL Lu^{3+} solution (1 mg L^{-1}, pH 7), and the Lu^{3+} concentration was measured at the same time points after chelation.

2.4 Cell Counting Kit-8 (CCK-8) Assay

CCK-8 assay was conducted using a PerkinElmer multimode microplate reader (PerkinElmer Inc., USA) to evaluate the cytotoxicity of Lu-PLA-g-PAO-Ms on HepG2 and LO2 cells. HepG2 and LO2 cells in the logarithmic growth phase were digested with trypsin to prepare single-cell suspensions, and the cell density was adjusted to 1×10^4 cells mL^{-1}. The cell suspension was seeded into 96-well cell culture plates at 100 μL per well, with medium-only wells set as blank controls. The plates were pre-incubated in a 5% CO2 humidified incubator at 37 ° C for 24 h to allow complete cell adhesion. After pre-incubation, the original medium was carefully discarded, and 100 μ L of complete medium containing Lu-PLA-g-PAO-Ms at different concentrations, 500 μg mL^{-1} $LuCl_3$ control solution, or blank complete medium was added to each well according to experimental groups. Each concentration was set with 6 replicates. After sample addition, the plate was gently tapped to mix, and incubation was continued under the same conditions. At 48 h and 72 h post-incubation, the plates were removed. CCK-8 reagent was mixed with DMEM basal medium at a 1:9 (v/v) ratio, and 100 μL of the mixture was added to each well under dark conditions to avoid bubble formation. After gentle mixing, the plates were returned to the incubator for 2 h of dark incubation at 37°C. Immediately after incubation, the absorbance values (OD) at 450 nm were measured using the microplate reader, and the raw data were recorded. The cell viability was calculated using the following formula:

$$\text{Cell viability (\%)} = \frac{(\mathrm{OD}_t - \mathrm{OD}_b)}{(\mathrm{OD}_c - \mathrm{OD}_b)} \times 100$$

where OD_b, OD_c, and OD_t represent the absorbance values of the blank control group, negative control group (blank complete medium), and experimental group, respectively. Statistical analysis of cell viability in each group was performed using GraphPad Prism 8.0 software to evaluate the effects of Lu-PLA-g-PAO-Ms at different concentrations and incubation times on the proliferation of HepG2 and LO2 cells.

2.5 Wound Healing Assay

Wound healing assay was performed using a Thermo Scientific EVOS M5000 inverted fluorescence microscope (Thermo Scientific, USA) to assess the effect of Lu-PLA-g-PAO-Ms on the migration ability of HepG2 cells. HepG2 cells in the logarithmic growth phase were prepared as a single-cell suspension at a density of 2.5×10^5 cells mL^{-1}, and seeded into 6-well cell culture plates at 2 mL per well. The plates were cultured under standard conditions until the cells formed a confluent monolayer with a fusion rate of over 90%. Two vertical straight scratches were uniformly made on the cell monolayer in each well using a sterile 200 μL pipette tip, keeping the tip vertical to avoid uneven scratch width, and the scratch position in each well was consistent. After scratching, the original medium was immediately discarded, and the wells were gently rinsed 3 times with sterile PBS to completely remove detached cells. Under the microscope, it was confirmed that the scratch edges were clear without residual floating cells. According to experimental groups, 2 mL of serum-free DMEM medium containing Lu-PLA-g-PAO-Ms at different concentrations was added to each well, with serum-free DMEM medium without microspheres as the blank control group. Each concentration was set with 3 replicates. Immediately after administration, the 6-well plate was placed under the inverted phase-contrast microscope, and images of fixed fields of each scratch were captured at 100× magnification to record the initial scratch width at 0 h. The plate was then returned to the incubator for continued culture, and images of the same fields at the same magnification were captured again at 24 h and 48 h post-incubation to record wound healing. ImageJ software was used to measure the scratch width at each time point, and the cell migration distance was calculated as follows: Migration distance = Initial scratch width - Scratch width at the corresponding time point. The migration distances of cells in each group at different time points were statistically analyzed to compare the effects of microspheres at different concentrations on the migration ability of HepG2 cells.

2.6 Calcein-AM/PI Live-Dead Cell Staining Assay

Calcein-AM/PI live-dead cell staining assay was carried out using a Thermo Scientific EVOS M5000 inverted fluorescence microscope (Thermo Scientific, USA) to visually evaluate the cytotoxicity of Lu-PLA-g-PAO-Ms. HepG2 cells in the logarithmic growth phase were prepared into single-cell suspensions with a cell density of 1×10^5 cells mL^{-1}, and seeded into 6-well plates at 1 mL per well. The plates were pre-incubated for 24 h in a 5% CO_2 humidified incubator at 37°C to allow cell adhesion. After pre-incubation, the original medium was discarded, and 1 mL of complete medium containing Lu-PLA-g-PAO-Ms at different concentrations was added to each well according to experimental groups, with complete medium without microspheres as the blank control group. Each concentration was set with 3 replicates, and the plates were incubated for 72 h under the same standard conditions.

At the end of incubation, the medium in each well was carefully collected into a sterile centrifuge tube. The cells were then gently rinsed twice with sterile PBS, and the rinse solution was also collected into the corresponding centrifuge tube to avoid losing floating cells. The collected medium and rinse solution were centrifuged at 1000 r min^{-1} for 3 min, and the supernatant was discarded. According to the instructions of the live-dead cell staining kit, 5 μL of concentrated Calcein-AM and PI staining solution were mixed thoroughly with 10 mL of PBS to prepare the staining working solution. 1 mL of the staining working solution was added to each centrifuge tube to resuspend the cell pellet, and the resuspended cell suspension was transferred back to the original corresponding cell culture well. The plate was shaken gently to ensure uniform contact between cells and the staining solution, and the cells were incubated in the dark at 37 °C for 15 min.

After incubation, dual-channel images of the same field were collected under the fluorescence microscope to observe the cell survival status, morphological changes, and death situation, so as to intuitively evaluate the cytotoxicity of the microspheres.

2.7 Coagulation Time Determination

Coagulation time determination was performed in 96-well plates to evaluate the effect of Lu-PLA-g-PAO-Ms on blood coagulation. Rabbit whole blood used in the experiment was collected in sodium citrate anticoagulant tubes. 50 μL of PBS, 50 μL of physiological saline (9 g L^{-1}), 50 μL of $CaCl_2$ solution (0.1 mol L^{-1}), and 50 μL of Lu-PLA-g-PAO-Ms physiological saline dispersions at different concentrations (50, 100, 250, 500, 1000 μg mL^{-1}) were added to consecutive wells of the 96-well plate, respectively. 50 μL of rabbit whole blood was added to each well. At 5, 10, 20, 30, and 60 min post-incubation, the coagulation process was terminated by rinsing the plate with physiological saline. The plate was repeatedly washed and the liquid was aspirated until the solution became clear (indicating that all soluble blood components had been removed). At the end of the experiment, the coagulation time and blood clot formation of each well were recorded.

2.8 Hemolysis Assay

Hemolysis assay was conducted using a multimode microplate reader to evaluate the hemocompatibility of Lu-PLA-g-PAO-Ms. 1 mL of rabbit whole blood was added to a centrifuge tube and centrifuged at 1500 rpm for 5 min. The supernatant was discarded, and 5–10 times the volume of physiological saline was added to the precipitate. The above centrifugation and washing steps were repeated 3 times to prepare red blood cell suspension (RCS). Eight 1.5 mL centrifuge tubes were prepared, and 1 mL of PBS, 1 mL of physiological saline, 1 mL of ultrapure water, and 1 mL of Lu-PLA-g-PAO-Ms physiological saline dispersions at different concentrations (50, 100, 250, 500, 1000 μg mL^{-1}) were added to the tubes, respectively. 20 μL of RCS was added to each centrifuge tube, and the tubes were incubated in a constant temperature incubator at 37 °C for 2 h. After incubation, the supernatant was aspirated from each tube and added to six wells of a 96-well plate (100 μL per well). The absorbance (OD) at 540 nm was measured using a microplate reader. The hemolysis rate was calculated using the following formula:

$$\text{Hemolysis rate (\%)} = \frac{(\mathrm{OD}_q - \mathrm{OD}_n)}{(\mathrm{OD}_p - \mathrm{OD}_n)} \times 100$$

where OD_q, OD_p, and OD_n represent the absorbance values of the Lu-PLA-g-PAO-Ms dispersion group, positive control group (ultrapure water group), and negative control group (physiological saline group), respectively.

2.9 Experimental Animals and Establishment of Orthotopic N1S1 Hepatocellular Carcinoma (HCC) Rat Model

Specific pathogen-free (SPF) female Sprague-Dawley (SD) rats (100–120 g) were selected as the experimental animals and housed in a clean environment of the Laboratory Animal Center. Rat hepatocellular carcinoma N1S1 cells were cultured *in vitro*, and the cells were collected when the proliferation concentration reached approximately 1×10^6 cells mL^{-1}. The collected cells were rinsed three times with PBS, and the cell concentration was adjusted to 5×10^7 cells mL^{-1} to prepare a cell suspension, which was stored on ice for subsequent use.

Rats were anesthetized by intraperitoneal injection of 100 μL of 3% sodium pentobarbital solution. After complete anesthesia, the rats were fixed on the operating table, and abdominal hair was removed with depilatory cream, followed by disinfection of the abdominal skin with iodophor. A transverse incision was made below the xiphoid process with sterile ophthalmic scissors to expose the liver, and the left outer lobe of the liver was gently pulled out of the abdominal cavity with a sterile cotton swab. A 100 μL aliquot of the prepared N1S1 cell suspension was aspirated with an insulin needle and slowly injected into the intrahepatic subcapsular region of the exposed liver parenchyma. After injection, the needle hole was pressed with a cotton swab to prevent cell suspension leakage, and then the syringe was withdrawn. The liver was returned to the abdominal cavity after confirming no bleeding at the needle hole, and the surgical wound was sutured and fully disinfected before the rats were placed back into the breeding cages for routine rearing. Magnetic resonance imaging (MRI) was performed on a 9.4 T small animal MRI scanner at 3 days post-modeling to monitor tumor engraftment, and successful orthotopic HCC model establishment was confirmed by MRI imaging results.

2.10 Grouping and Hepatic Artery Administration of Therapeutic Agents

Rats with successfully engrafted orthotopic liver tumors (tumor volume approximately 15 mm^3) were randomly divided into four experimental groups with 6 rats per group: normal saline (NS) control group, $^{177}LuCl_3$ group, blank PLA-g-PAO microspheres (PLA-g-PAO-Ms) group, and ^{177}Lu-labeled PLA-g-PAO microspheres (^{177}Lu-PLA-g-PAO-Ms) group. All therapeutic agents were administered via hepatic artery intervention, and the specific operational steps were as follows: rats were anesthetized with 3% sodium pentobarbital as described above; the abdominal cavity was opened, and the abdominal artery, hepatic artery, and gastroduodenal artery were gently separated with sterile cotton swabs and forceps; two ligators were placed around the gastroduodenal artery, with the distal end ligated, and a ligator was placed around the abdominal artery for temporary blood flow interruption; a self-made needle was used to puncture the gastroduodenal artery at the upstream of the distal ligation site, and a catheter was inserted into the hepatic artery for agent injection.

The administration dosage for each group was strictly controlled as 100 μL per rat: the NS group was injected with 100 μL of physiological saline; the $^{177}LuCl_3$ group with 100 μL of $^{177}LuCl_3$ solution (11.1 MBq); the blank PLA-g-PAO-Ms group with 100 μL of PLA-g-PAO-Ms suspension (20 mg mL^{-1}); the ^{177}Lu-PLA-g-PAO-Ms group with 100 μL of ^{177}Lu-PLA-g-PAO-Ms formulation (20 mg mL^{-1}, 11.1 MBq). After agent injection, the proximal end of the gastroduodenal artery (upstream of the puncture site) was ligated, the ligator around the abdominal artery was removed to restore hepatic artery blood flow, and the abdominal cavity was sutured and disinfected.

2.11 *In vivo* Imaging and Tumor Volume Dynamic Monitoring

Single-photon emission computed tomography/computed tomography (SPECT/CT) imaging was performed on a nanoScan SPECT/CT scanner at 7 and 14 days post-administration to evaluate the *in vivo* biological distribution and radiostability of ^{177}Lu-PLA-g-PAO-Ms. Dynamic MRI monitoring was conducted on the 9.4 T small animal MRI scanner at 7 and 14 days post-administration to assess the tumor growth response to different interventions. Tumor volume was calculated using the formula: $V (mm^3) = (L \times S^2)/2$, where L represents the maximum diameter of the tumor and S represents the minimum diameter of the tumor, with tumor size measured from the MRI imaging results.

2.12 Biodistribution Analysis of Radionuclides

All experimental rats were euthanized at 14 days post-administration for biodistribution analysis. Rats from the $^{177}LuCl_3$ group and ^{177}Lu-PLA-g-PAO-Ms group were selected for tissue collection: heart, liver, spleen, lung, kidney, stomach, intestine, bone, muscle, skin, and tumor tissues were carefully dissected, placed in sterile plastic test tubes, and weighed immediately. The residual radioactive concentration of each tissue sample was detected using a γ-counter, and the radioactive uptake level was calculated as the percentage of injected dose per gram of tissue (%ID g^{-1}) to quantify the *in vivo* distribution of ^{177}Lu.

All animal experiments were performed in compliance with the standard laboratory animal care protocols, and the experimental procedures were designed to ensure reproducibility with detailed operational specifications.

All experimental data were processed and plotted using Origin 2021 and GraphPad Prism 8.0 software. Statistical analysis was performed with an unpaired two-tailed Student's t-test for two-group comparisons of continuous variables and Kruskal-Wallis ANOVA with Dunn's multiple comparison test for multiple-group comparisons, with data expressed as mean ± standard deviation (SD) and $p < 0.05$ considered statistically significant. XPS spectral data were specifically fitted and analyzed using Thermo Avantage software.

3 RESULTS AND DISCUSSION

3.1 Synthesis and Characterization of PLA-g-PAO-Ms

PLA-g-PAO-Ms were generated through three-steps involving the preparation of PLA-Ms by microfluidic technology, surface functionalization via electron beam-induced graft polymerization, and amidoximation modification (Fig. 1). The microfluidic process yielded microspheres with uniform size distribution and regular morphology. The relevant preparation parameters have been systematically optimized in our previous studies. Electron-beam-induced graft polymerization was used to introduce nitrile-containing chains onto the surface of PLA-Ms under room-temperature, additive-free conditions. Subsequent amidoximation converted these nitrile groups into amidoxime ligands, yielding the target PLA-g-PAO-Ms and providing coordination sites for radiometal binding. FT-IR confirmed the stepwise surface modification (Fig. 2a).For PLA-Ms, the characteristic peaks observed at 1082 cm^{-1} and 1748 cm^{-1} are assigned to the symmetric stretching vibration of the C-O-C ether bond and the stretching vibration of the ester carbonyl (C=O) group, respectively.[17] After irradiation-induced grafting, a new characteristic peak emerged at 2243 cm^{-1} in the FT-IR spectrum of PLA-g-PAN-Ms, which is attributed to the stretching vibration of the cyano (C≡N) group, confirming that acrylonitrile was successfully grafted onto the surface of the microspheres. After the amidoximation reaction, the characteristic cyano peak at 2243 cm^{-1} in the FT-IR spectrum of PLA-g-PAO-Ms completely disappeared. Meanwhile, new absorption peaks appeared at 3401 cm^{-1}, 1647 cm^{-1} and 922 cm^{-1}, which correspond to the stretching vibration of N-H bond, the stretching vibration of C=N bond, and the bending vibration of N-O bond in the amidoxime group, respectively, verifying the successful introduction of the target functional groups.[18] XPS analysis further confirmed the completion of grafting modification and amidoximation reaction. The N 1s characteristic peak at 399.1 eV was observed in the full survey XPS spectra of both PLA-g-PAN-Ms and

PLA-g-PAO-Ms, while no such signal was detected in pristine PLA-Ms, indicating that nitrogen-containing groups were successfully introduced onto the microsphere surface via the grafting reaction. The high-resolution N 1s spectrum of PLA-g-PAO-Ms was subjected to deconvolution fitting, and three characteristic peaks were fitted with binding energies at 399.33 eV, 399.84 eV and 400.88 eV, which are assigned to C-NH, $C-NH_2$ and C=N bonds, respectively (Fig. 2b and c). The high-resolution C 1s spectrum further confirmed the presence of chemical structures including O-C-O, -CN, C-H and C=C (Fig. S1a, Supporting Information). XPS analysis was performed on PLA-g-PAO-Ms after Lu^{3+} chelation, and the characteristic double peaks of Lu $4d_{5/2}$ and Lu $4d_{3/2}$ were observed at 197.48 eV and 206.43 eV, which confirmed the coordination binding between Lu^{3+} and the amidoxime groups on the microsphere surface (Fig. 2d).

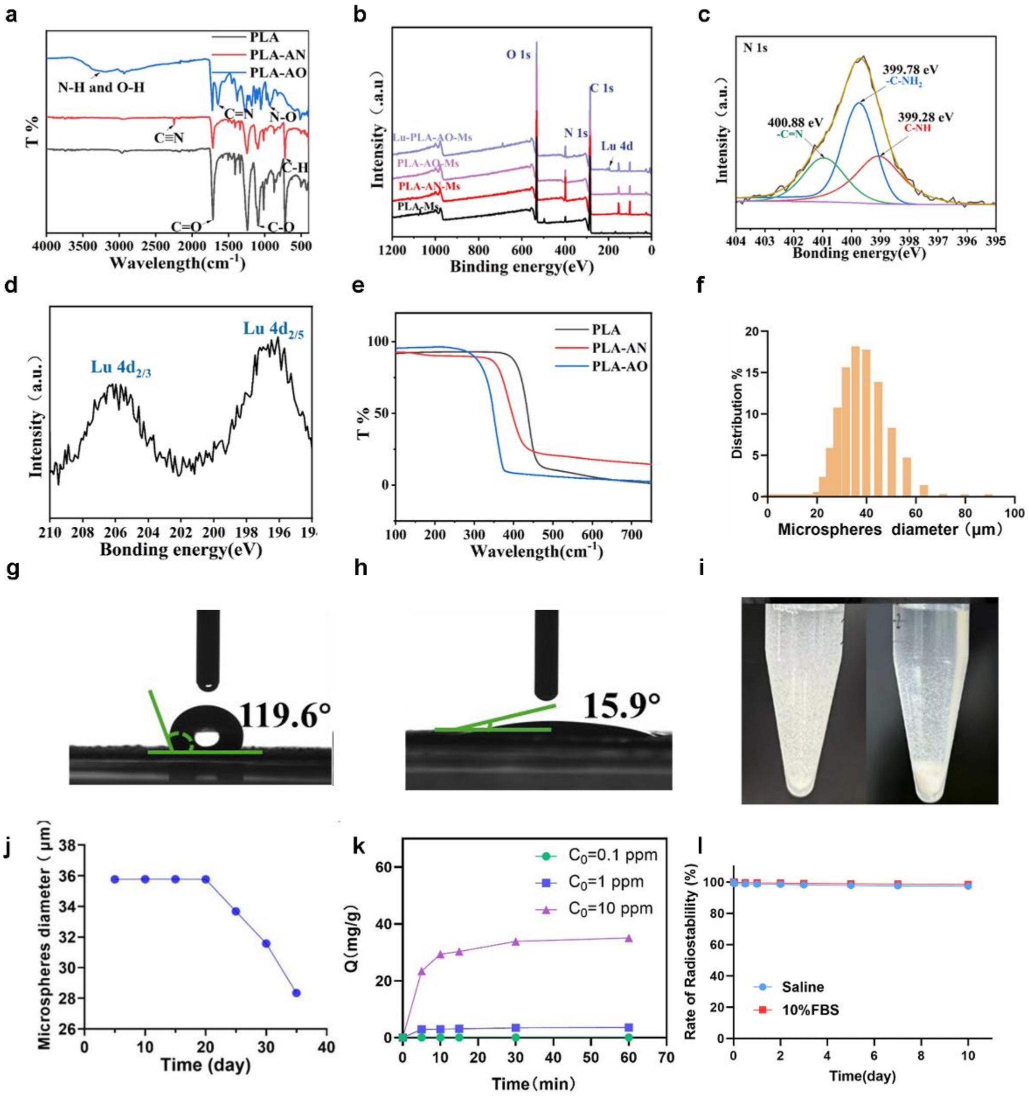

Fig. 2 Physicochemical and functional characterization of the microspheres. (a) FT-IR spectra of PLA-Ms, PLA-g-PAN-Ms, and PLA-g-PAO-Ms;(b) XPSsurvey spectra of PLA-Ms, PLA-g-PAN-Ms, PLA-g-PAO-Ms, and Lu-loaded PLA-g-PAO-Ms (Lu-PLA-g-PAO-Ms);(c) High-resolution N 1s XPS spectrum of Lu-PLA-g-PAO-Ms;(d) High-resolution Lu 4d XPS spectrum of Lu-PLA-g-PAO-Ms;(e) TGA curves of PLA-Ms, PLA-g-PAN-Ms, and PLA-g-PAO-Ms;(f) Particle size

distribution curve of PLA-g-PAO-Ms;(g) Static water contact angle profile of PLA-Ms;(h) Static water contact angle profile of PLA-g-PAO-Ms;(i) Optical photograph of the dispersibility of PLA-Ms and PLA-g-PAO-Ms in aqueous solution;(j) Particle size variation curve of PLA-g-PAO-Ms during *in vitro* degradation;(k) Time-dependent Lu^{3+} loading capacity of PLA-g-PAO-Ms at different initial Lu^{3+} concentrations;(l) *In vitro* radiochemical stability of ^{177}Lu-PLA-g-PAO-Ms.

TGA was performed to characterize the thermal stability changes of the microspheres during the stepwise modification (Fig. 2e). For pristine PLA-Ms, the T_{max} was determined to be 460 °C. After irradiation-induced graft polymerization, a distinct decrease in Tmax to 330 °C was observed for the obtained PLA-g-PAN-Ms, corresponding to the successful grafting of acrylonitrile on the microsphere surface. Following the amidoximation modification, the thermal stability of the final product PLA-g-PAO-Ms further declined, with an onset decomposition temperature of approximately 180 °C. Although the stepwise surface modification reduced the overall thermal stability of the microspheres, the thermal degradation behavior of the PLA matrix backbone was not fundamentally altered, which still meets the thermal stability requirements for room-temperature radiolabeling and subsequent interventional therapy. SEM observations show that both PLA-Ms and PLA-g-PAO-Ms exhibit a regular spherical morphology and smooth surface structure (Fig. 3). Laser particle size analysis (wet dispersion mode) results show that the median particle size (D50) of PLA-g-PAO-Ms is 33.73±0.03 μm, with more than 90% of the microspheres presenting a particle size distribution in the range of 20–80 μm (Fig. 2f), which meets the particle size requirements of embolic microspheres for TARE therapy.[19] In addition, the dispersion test confirms that the microspheres can be stably dispersed in PBS without obvious aggregation (Fig. 2l). WCA tests showed that the WCA of PLA-g-PAO-Ms significantly decreased from 119.1° for PLA-Ms to 15.9° (Fig. 2g and h). The remarkable reduction in contact angle confirms that amidoximation modification can greatly improve the surface hydrophilicity of the microspheres. *In vitro* degradation assays of PLA-g-PAO-Ms were carried out in a 10% fetal bovine serum (FBS)-containing buffer system under physiological-mimicking conditions (37 °C, 100 rpm). As shown in Fig. 2(j), the as-prepared PLA-g-PAO-Ms initiated the degradation process on the 20th day of incubation, and achieved a mass loss rate of 72% (corresponding to 28% residual mass) at day 35. Given that the physical half-life of ^{177}Lu is 6.7 days, its radioactivity will decay to less than 5% of the initial level after 5 half-lives (approximately 33.5 days). Noteworthily, PLA-g-PAO-Ms maintained excellent structural integrity during the entire effective therapeutic irradiation window (the first 20 days after administration), which can effectively avoid premature leakage of the loaded radionuclide and its subsequent non-specific systemic distribution, thus guaranteeing the biosafety of the carrier during the whole treatment cycle. [20]

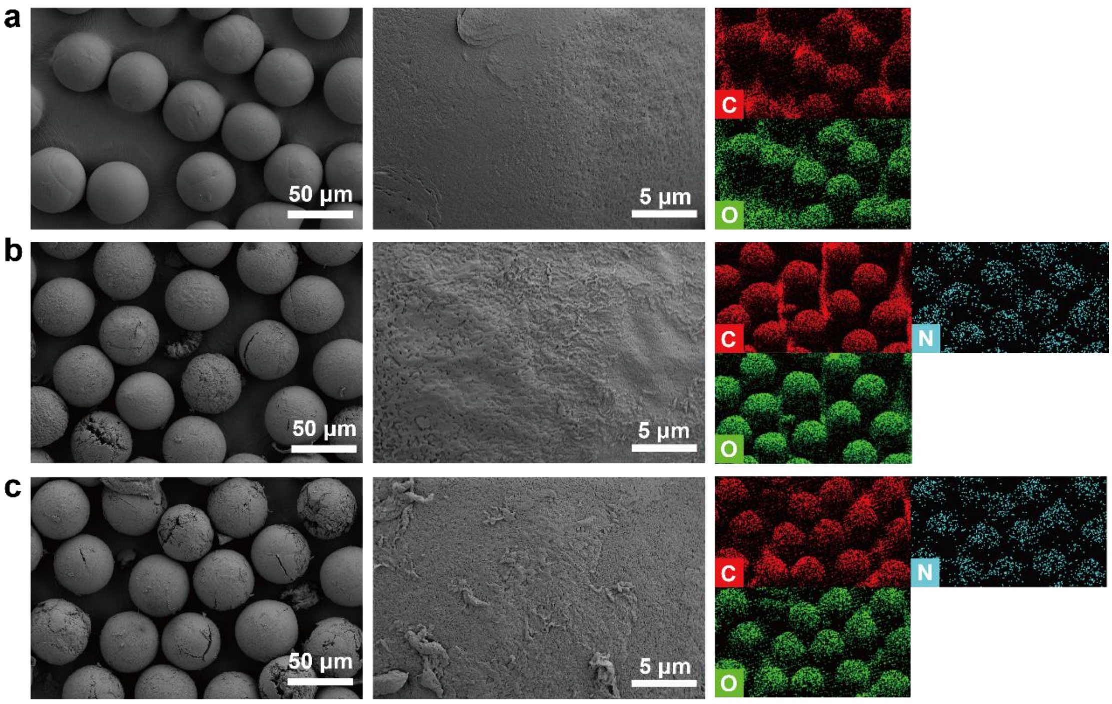

Fig. 3 SEM images and EDS mapping of PLA-Ms (a), PAN-g-PLA-Ms (b), and PAO-g-PLA-Ms (c).

To optimize the Lu^{3+} chelation efficiency of PLA-g-PAO-Ms, the effects of key parameters including solution pH, solid-to-liquid ratio, reaction time and initial Lu^{3+} concentration on the chelation capacity were systematically investigated. In the pH range of 5 to 9, the chelation capacity increased with increasing pH, with values of 2.19, 2.28, 2.32, 3.06 and 3.60 mg g^{-1}, respectively (Fig. S1b). The significantly improved chelation efficiency at pH 8–9 can be attributed to two factors: first, the formation of a $Lu(OH)_3$ precipitate can be avoided at pH < 9; second, the deprotonation degree of amidoxime groups increases under alkaline conditions, which enhances their chelating affinity for Lu^{3+} ions. Kinetic studies under different pH conditions showed that the chelation capacity increased with prolonged reaction time and reached equilibrium within 30 minutes (Fig. S1c). The equilibrium chelation capacities at pH 5, 7 and 9 were 2.20, 2.32 and 3.60 mg g^{-1}, respectively, with corresponding Lu^{3+} utilization efficiencies of 44.6%, 47.2% and 73.1%, respectively. Solid-to-liquid ratio optimization experiments showed that the Lu^{3+} chelation capacity per unit mass of microspheres increased correspondingly with decreasing solid-to-liquid ratio (0.1, 0.5 and 2 mg mL^{-1}) (Fig. S1d), and chelation equilibrium was reached within 30 minutes for all groups. The chelation capacity of PLA-g-PAO-Ms exhibited a positive correlation with the initial Lu^{3+} concentration (Fig. 2k). When the Lu^{3+} concentrations were 0.1, 1 and 10 ppm, the corresponding equilibrium chelation capacities were 0.12, 3.49 and 33.83 mg g^{-1}, respectively.

The reported specific activity of good manufacturing practice (GMP)-grade ^{177}Lu varies with the production reactor, ranging from approximately 740 to 2960 GBq mg^{-1}.[21] Based on the maximum chelation capacity (33.83 mg g^{-1}) measured in this study and the above clinical specific activity data, the theoretical ^{177}Lu radioloading capacity of 1 mg PLA-g-PAO-Ms can reach 24.7–98.8 GBq, which fully meets the requirements for a single clinical therapeutic dose (0.5–3 GBq). In comparison, the radioloading capacity of commercially available clinical-grade ^{90}Y glass microspheres is approximately

0.05–0.1 GBq mg^{-1}, while that of resin microspheres is only 0.002 GBq mg^{-1}, indicating that PLA-g-PAO-Ms have significant advantages in radionuclide loading capacity. *In vitro* stability studies of ^{177}Lu-PLA-g-PAO-Ms in PBS and 10% FBS showed that the ^{177}Lu retention rates in both media were above 98.9% after 10 days of incubation at 37 °C (Fig. 2l). The above results indicate that ^{177}Lu-PLA-g-PAO-Ms exhibit excellent radiochemical stability and physiological stability, ensuring the continuous and stable emission of radiation energy from ^{177}Lu during TARE therapy, which lays a critical foundation for its clinical translation. In summary, we successfully fabricated PLA-g-PAO-Ms with well-defined structure and controllable performance, which exhibit high Lu^{3+} chelation capacity and excellent labeling stability, providing a qualified carrier material for subsequent biological evaluation. [20, 22]·[23]

3.2 Cytocompatibility and Hemocompatibility of Lu-PLA-g-PAO-Ms

Cytocompatibility is a core metric for evaluating the biosafety of carrier materials used in TARE. [24] To systematically assess the cytocompatibility of Lu-PLA-g-PAO-Ms, HCC HepG2 cells and human normal hepatic LO2 cells were selected as *in vitro* models, and comprehensive analysis was performed using a battery of assays including plate colony formation assay, CCK-8 proliferation assay, scratch wound healing assay, and live/dead cell staining assay. The results of the plate colony formation assay showed no significant differences in the colony number and morphological characteristics of HepG2 cells between the control group and groups treated with gradient doses of Lu-PLA-g-PAO-Ms, with no statistically significant difference ($p>0.05$, Fig. 4a and b). Colony formation ability reflects the long-term proliferation potential and self-renewal capacity of cells. The above results indicated that the microspheres exerted no inhibitory effect on the colony formation process of HepG2 cells within the tested dose range, suggesting that the matrix material of the microspheres did not significantly interfere with cell proliferation behavior, providing an experimental basis for subsequent *in vivo* safety assessment.

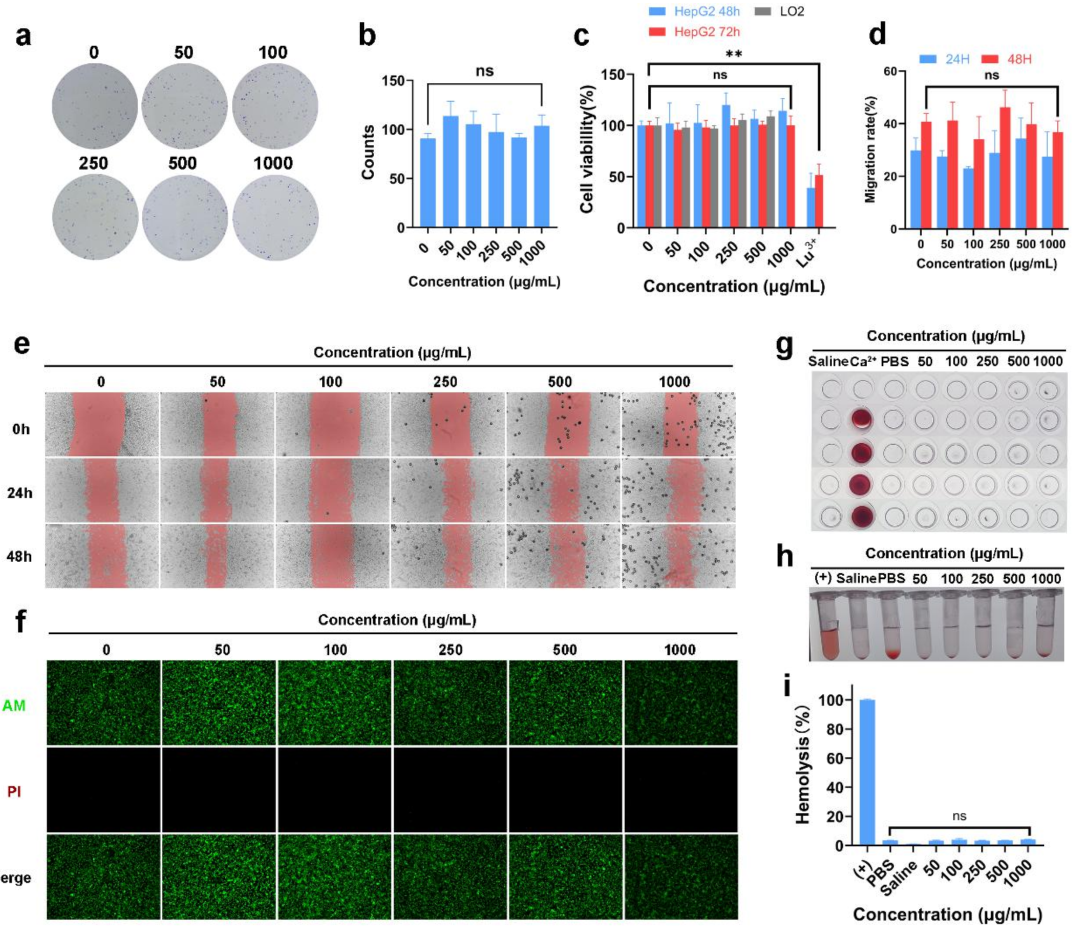

Fig. 4 Experimental results obtained under different concentrations of Lu-PLA-g-PAO-Ms: (a) Representative images of colony formation assay; (b) Quantitative statistical analysis of colony formation assay; (c) Quantitative statistical results of CCK-8 cell viability assay; (d) Quantitative analysis of cell migration rate from scratch wound healing assay; (e) Representative images of scratch wound healing (cell migration) assay; (f) Representative images of live/dead cell viability staining assay; (g) Results of *in vitro* blood coagulation assay; (h) Visual images of hemolysis assay; (i) Quantitative statistical analysis of hemolysis assay.

The CCK-8 proliferation assay further confirmed the favorable cytocompatibility of the microspheres. After LO2 cells were co-cultured with different concentrations of Lu-PLA-g-PAO-Ms for 72 h, the cell viability of each group exceeded 90%; the viability of HepG2 cells also remained above 90% at 48 h and 72 h, with no statistically significant difference from the control group (p>0.05, Fig. 4c). As a control, treatment with free Lu^{3+} (50 $mg·L^{-1}$ $LuCl_3$) for 72 h significantly reduced the viability of HepG2 cells to 51.4% (p<0.001). This result was consistent with the conclusion from the *in vitro* release assay of Lu-PLA-g-PAO-Ms that the microspheres can stably chelate Lu element, indicating that Lu-PLA-g-PAO-Ms exhibited favorable *in vitro* cytocompatibility and providing preliminary experimental support for subsequent *in vivo* biosafety evaluation.

The scratch wound healing assay showed no significant difference in cell migration rates between the control group and groups treated with different concentrations of Lu-PLA-g-PAO-Ms at 24 h and 48 h (p>0.05, Fig. 4d and e), suggesting that the microspheres did not affect the intrinsic migratory capacity of HepG2 cells. The live/dead staining results further supported the above conclusion. After co-culturing with different concentrations of microspheres for 48 h and 72 h, the cell population was dominated by Calcein-AM-positive (green, viable) cells, while PI-positive (red, dead) cells were extremely rare (Fig. 4f), with no evidence of impaired cell membrane integrity.

Multiple *in vitro* assays, including plate colony formation assay, CCK-8 proliferation assay, scratch wound healing assay, and live/dead cell staining, consistently demonstrated that Lu-PLA-g-PAO-Ms exhibited favorable cytocompatibility within the tested dose range.

Given that embolic carriers are in direct contact with blood during clinical TARE procedures, hemocompatibility is a prerequisite for their translational application.[25] The hemocompatibility of Lu-PLA-g-PAO-Ms was systematically evaluated by measuring the *in vitro* coagulation time and hemolysis rate using whole blood from New Zealand White rabbits (all animal experimental procedures were approved by the Institutional Animal Care and Use Committee (IACUC) of our institution). The coagulation assay showed that after co-incubation of microsphere suspensions at different concentrations with rabbit whole blood, there was no statistically significant difference in coagulation time between each experimental group and the normal saline (NS) control group (p>0.05, Fig. 4g), indicating that Lu-PLA-g-PAO-Ms did not activate the coagulation system. The hemolysis assay showed that after co-incubation of microspheres at different concentrations with rabbit erythrocytes at 37°C for 2 h, the supernatant of each group was clear and transparent (Fig. 4h), and the hemolysis rate of each group was below 5% (Fig. 4i), meeting the requirements of ISO 10993-4 for blood-contacting materials.[26] The favorable hemocompatibility can effectively prevent microsphere-induced adverse reactions such as thrombosis and hemolysis, ensure successful embolization of the microspheres into the tumor microvasculature, and guarantee the safety of TARE procedures.

3.3 Radiostability and efficacy of ^{177}Lu-PLA-g-PAO microspheres

Due to the well-validated excellent *in vitro* performance of ^{177}Lu-PLA-g-PAO-Ms, we constructed an orthotopic N1S1 HCC rat model to validate the *in vivo* radiostability, tumor targeting capability, and anti-tumor therapeutic efficacy of ^{177}Lu-PLA-g-PAO-Ms (Fig. 5a). The orthotopic HCC rat model was established via intrahepatic subcapsular injection of N1S1 cells, and successful tumor engraftment was confirmed by MRI. Tumor-bearing rats were randomly divided into four groups (n = 6 per group): NS control group, ^{177}LuCl$_3$ solution group, blank PLA-g-PAO-Ms embolization group, and ^{177}Lu-PLA-g-PAO-Ms treatment group, with all interventions administered via the hepatic artery. SPECT/CT imaging was performed on day 7 and day 14 post-treatment to evaluate the *in vivo* distribution and radiostability of the microspheres (Fig. 5d). Representative SPECT/CT images of the ^{177}LuCl$_3$ group showed a significant systemic spread of radioactive signals throughout the body over time, with predominant ^{177}Lu accumulation in the skeleton. Conversely, representative SPECT/CT images of the ^{177}Lu-PLA-g-PAO-Ms group showed that radioactive signals were highly restricted to the tumor lesions, with no detectable off-target radionuclide migration observed at both day 7 and day 14 post-administration. This indicates that ^{177}Lu-PLA-g-PAO-Ms possess excellent *in vivo* radiostability and tumor targeting capability, which is attributed to the stable chelation of PLA-g-PAO-Ms with ^{177}Lu, effectively hindering the off-target diffusion of radionuclides and reducing the risk of unnecessary radiation exposure to non-target organs and tissues. MRI was performed on day 7 and day 14 post-treatment to monitor the tumor response to different interventions (Fig. 5b). Quantitative MRI analysis showed that tumors in the NS control group and ^{177}LuCl$_3$ group grew continuously over the observation period; although a mild inhibitory trend was observed in the ^{177}LuCl$_3$ group, the difference did not reach statistical significance ($p>0.05$). Treatment with blank PLA-g-PAO-Ms only partially inhibited tumor growth compared with the NS control and ^{177}LuCl$_3$ groups, which is attributed to the embolization effect of PLA-g-PAO-Ms that blocks the tumor blood supply, thereby slowing down tumor growth. Notably, ^{177}Lu-PLA-g-PAO-Ms yielded a more remarkable anti-tumor effect, with significant tumor growth suppression and even partial tumor regression observed on day 14 post-treatment, exhibiting superior therapeutic efficacy compared with the blank embolization-only group. The tumor volumes in both the blank PLA-g-PAO-Ms group and ^{177}Lu-PLA-g-PAO-Ms group were significantly smaller than those in the NS control group on day 14 post-treatment ($p<0.001$).

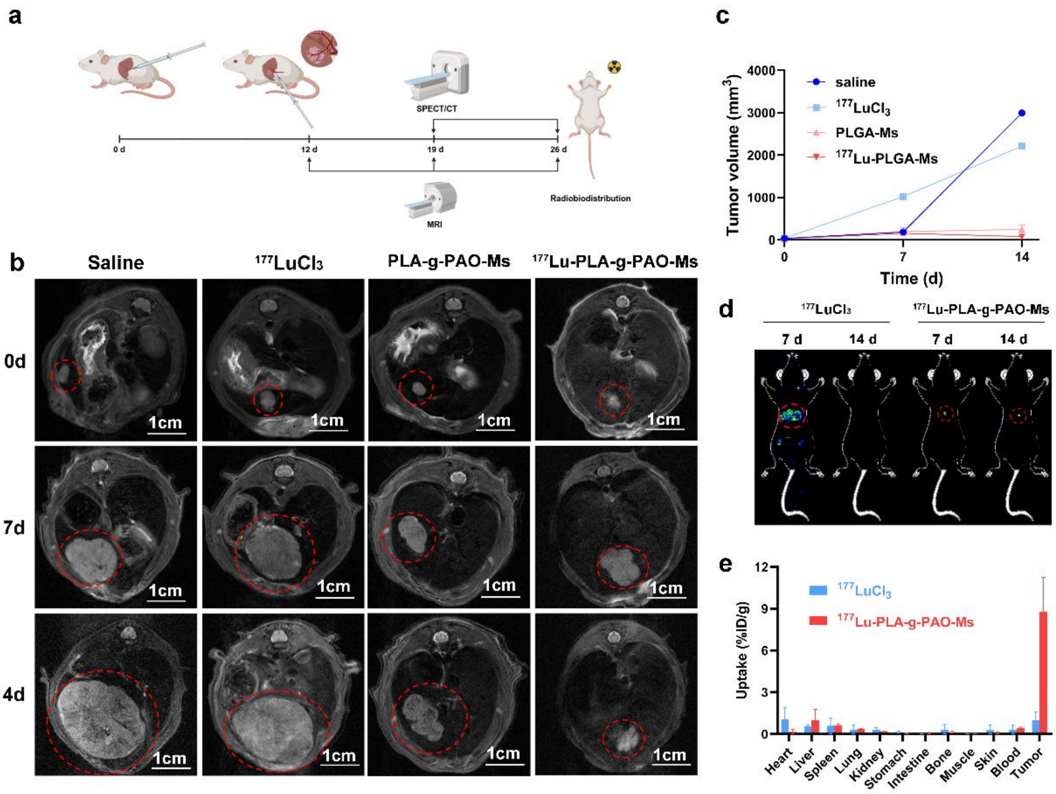

Fig. 5 Antitumor efficacy and *in vivo* biological behavior evaluation after hepatic artery administration in rat N1S1 orthotopic hepatocellular carcinoma models. (a) Schematic diagram of the hepatic artery administration procedure and post-treatment evaluation workflow, outlining the establishment strategy of rat orthotopic hepatocellular carcinoma model, the experimental grouping scheme for hepatic artery administration, as well as the serial imaging evaluation and biological detection procedures after administration. Created in https://BioRender.com (b) MRI images of tumors in the Saline group, ^{177}LuCl$_3$ group, PLA-g-PAO-Ms group, and ^{177}Lu-PLA-g-PAO-Ms group on day 0, day 7, and day 14 after administration. Red circles indicate the tumor boundaries. (c) Tumor growth curves of the above four experimental groups after administration. (d) Representative SPECT images of the ^{177}LuCl$_3$ group and ^{177}Lu-PLA-g-PAO-Ms group on day 5 and day 10 after

administration. Red circles indicate the tissue uptake sites of ^{177}Lu. (e) *In vivo* biodistribution profile of the ^{177}LuCl₃ group and ^{177}Lu-PLA-g-PAO-Ms group in rat N1S1 orthotopic hepatocellular carcinoma models at 14 days after hepatic artery administration.

Biodistribution analysis performed on day 14 post-treatment further verified the *in vivo* SPECT/CT imaging results (Fig. 5e). The biodistribution results showed that tumor tissues in the ^{177}Lu-PLA-g-PAO-Ms group exhibited the highest radioactive uptake, reaching 8.79 ± 1.74 %ID g^{-1}, with radioactive counts significantly higher than those in normal liver tissue (1 ± 0.54 %ID g^{-1}) and other normal organs and tissues including the heart (0.15 ± 0.11 %ID g^{-1}), spleen (0.65 ± 0.06 %ID g^{-1}), lung (0.38 ± 0.03 %ID g^{-1}), kidney (0.22 ± 0.002 %ID g^{-1}), and blood (0.45 ± 0.03 %ID g^{-1}) ($p<0.001$). In contrast, the radioactive uptake values of other non-target organs and tissues in the ^{177}Lu-PLA-g-PAO-Ms group remained at an extremely low level, causing no severe radiation damage to normal tissues. However, the ^{177}LuCl₃ group showed only 0.30 ± 0.28 %ID g^{-1} of radioactive uptake in tumor tissues, with systemic distribution of radionuclides and significant accumulation in non-target organs, especially the bone, kidney and spleen. This was mainly attributed to the rapid clearance and non-specific protein binding of ^{177}Lu, leading to non-targeted retention in normal organs. Therefore, ^{177}Lu-PLA-g-PAO-Ms can effectively avoid off-target radiation damage to normal tissues *in vivo*, and greatly improve the effectiveness and biosafety of *in vivo* TARE applications.

4 CONCLUSIONS

This work focuses on the critical material challenges encountered in the clinical application of TARE. Currently, clinically used radioactive microspheres generally have inherent limitations including non-degradability, insufficient radionuclide labeling stability, and lack of integrated theranostic capability. To address these issues, we developed PLA-g-PAO-Ms, and systematically evaluated their physicochemical properties, biosafety, and *in vivo* anti-tumor efficacy as a ^{177}Lu-labeled carrier for TARE. Our results demonstrate that the amidoxime coordination sites on the microsphere surface enable efficient and stable chelation of ^{177}Lu, with a degradation behavior well matched to the physical half-life of ^{177}Lu. This system maintains excellent biocompatibility while exhibiting a significant tumor growth inhibitory effect in hepatocellular carcinoma models. These findings indicate that PLA-g-PAO-Ms provide a novel material design strategy and experimental basis for the construction of biodegradable multifunctional radionuclide carriers for TARE therapy. In terms of preparation methodology, we established a fabrication strategy combining microfluidic fabrication, electron beam irradiation-induced grafting, and amidoximation functionalization, which addresses key technical bottlenecks in the traditional preparation process of radioactive microspheres to a certain extent. Microfluidic technology enables precise regulation of the particle size and morphology of the microspheres. The obtained PLA-g-PAO-Ms have a median particle size of 33.73±0.03 μm, with approximately 90% of the microspheres distributed in the size range of 20 to 80 μm, which meets the basic requirements for embolic microspheres in TARE therapy, while simultaneously balancing catheter deliverability and tumor microvascular embolization efficiency. Compared with traditional radionuclide labeling methods relying on reactor neutron activation, we adopted electron beam-induced graft polymerization to construct functional sites on the microsphere surface. This approach achieves controllable modification of the material surface under relatively mild conditions and avoids significant damage to the polymer chain structure. This method does not require the additional introduction of chemical initiators, which reduces the risk of impurity introduction to a certain extent, while preserving the inherent physicochemical properties and degradation characteristics of the polylactic acid matrix. Material characterization results further confirm that amidoxime groups can be stably anchored on the microsphere surface and provide effective coordination sites, offering a structural foundation for the stable chelation of radionuclides and thereby improving the stability of radionuclide labeling. Biodegradability is a key feature that distinguishes this carrier from clinically available non-degradable ^{90}Y microspheres, with its degradation process rationally designed to balance both therapeutic efficacy and biosafety. *In vitro* degradation experiments show that PLA-g-PAO-Ms initiate obvious degradation on approximately day 20 in a simulated physiological environment, with a mass loss rate reaching 72% by day 35. This degradation profile is well matched to the physical half-life of ^{177}Lu. After approximately 3 half-lives of ^{177}Lu (around day 20), its radioactivity has dropped to below 12.5% of the initial value, with the treatment-related radiation energy essentially fully released, at which point the microspheres undergo gradual degradation. This characteristic maintains the structural stability of the microspheres during the radiotherapy window period, thereby reducing the risk of systemic off-target toxicity caused by premature radionuclide release. Meanwhile, it avoids long-term retention of the microspheres in liver tissue, reduces the incidence of potential complications such as long-term vascular stenosis and chronic inflammation, and reserves a certain safety margin for subsequent repeated TARE treatments that may be required. [90]The amidoxime groups on the surface of PLA-g-PAO-Ms endow the material with strong radionuclide chelating capacity and lay a foundation for functional expansion. Experimental results show that the maximum chelating capacity of the microspheres for Lu^{3+} can reach 33.83 mg g^{-1}. Estimated based on the specific activity of clinical-grade ^{177}Lu, its theoretical radioloading capacity can meet the dose requirements of a single TARE treatment, and exhibits high drug loading potential. Stability evaluation results demonstrate that the radionuclide retention rate of ^{177}Lu-labeled microspheres remains above 98.9% after 10 days of incubation in physiological media. *In vivo* SPECT/CT imaging and 14-day biodistribution study both confirm that the radionuclide can be stably retained in the tumor lesion area, with no obvious off-target migration observed, which verifies the stability of the labeling system at both *in vitro* and *in vivo* levels. Compared with the limitation of mainstream clinical ^{90}Y microspheres that lack real-time imaging capability, the gamma rays emitted by ^{177}Lu enable non-invasive visualized monitoring during the treatment process via SPECT/CT. Meanwhile, the strong coordination ability of amidoxime groups towards a variety of transition metal radionuclides endows the microspheres with the potential to further construct a co-labeling system of therapeutic and imaging radionuclides, providing new possibilities for the optimization of TARE treatment strategies in different clinical scenarios.

From the perspective of clinical translation, the ^{177}Lu-labeled PLA-g-PAO-Ms developed in this work provide a promising candidate carrier for transarterial radioembolization of unresectable hepatocellular carcinoma. There remains a significant unmet therapeutic need for patients with intermediate and advanced hepatocellular carcinoma at present. Clinically used radioactive microspheres have certain limitations in their safety and applicable scope to a certain extent due to their non-degradability and potential risk of radionuclide leakage. On the basis of preserving the synergistic effect of embolization and internal irradiation of TARE technology, the biodegradable microspheres prepared in this study overcome several limitations of existing carrier materials. The material exhibits excellent biocompatibility, stable radionuclide retention capacity, and definite *in vivo* tumor inhibitory effect, which lays an experimental foundation for subsequent preclinical evaluation in large animal models and systematic toxicological studies, and also provides a new material option for further optimization of treatment strategies for unresectable hepatocellular carcinoma. This study still has certain limitations that need to be further addressed in subsequent work. First, this study only completed the short-term efficacy and safety evaluation in a rat N1S1 orthotopic hepatocellular carcinoma model, and has not yet been validated in large animal models that more closely mimic the clinical application scenario. The rabbit VX2 hepatocellular carcinoma model or canine normal liver model can better simulate the conditions of clinical interventional procedures, and have important reference value for evaluating catheter deliverability, dosimetry distribution, and long-term safety. Second, this study has not performed a direct comparison with widely used clinical commercial ^{90}Y microspheres, thus lacking a systematic assessment of the differences in efficacy and safety between the two. Third, this study mainly verified the chelation and therapeutic efficacy of ^{177}Lu, while the labeling efficiency and *in vivo* performance of the amidoxime coordination structure for other common TARE radionuclides such as ^{166}Ho or ^{90}Y still need further investigation. Finally, the *in vivo* observation period of this study was 14 days, and systematic data on the histological response, chronic inflammation, and long-term systemic toxicity that may occur during the complete *in vivo* degradation cycle of the microspheres are still lacking.

This study still has certain limitations that need to be further addressed in subsequent work. First, this study only completed the short-term efficacy and safety evaluation in a rat N1S1 orthotopic hepatocellular carcinoma model, and has not yet been validated in large animal models that more closely mimic the clinical application scenario. The rabbit VX2 hepatocellular carcinoma model or canine normal liver model can better simulate the conditions of clinical interventional procedures, and have important reference value for evaluating catheter deliverability, dosimetry distribution, and long-term safety. Second, this study has not performed a direct comparison with widely used clinical commercial ^{90}Y microspheres, thus lacking a systematic assessment of the differences in efficacy and safety between the two. Third, this study mainly verified the chelation and therapeutic efficacy of ^{177}Lu, while the labeling efficiency and *in vivo* performance of the amidoxime coordination structure for other common TARE radionuclides such as ^{166}Ho or ^{90}Y still need further investigation. Finally, the *in vivo* observation period of this study was 14 days, and systematic data on the histological response, chronic inflammation, and long-term systemic toxicity that may occur during the complete *in vivo* degradation cycle of the microspheres are still lacking.

Author contributions

J.L. and H.M. provided Conceptualization and secured Funding acquisition. X.L., G.W., and X.X. contributed to Methodology. X.L., G.W., Z.Z., and H.C. conducted the Investigation. X.L. performed Formal analysis. G.W. undertook Data curation. Z.Z. completed Visualization. H.W. provided Validation. X.X. offered Resources and Supervision, and H.M. also provided Supervision. X.L. prepared the Writing – original draft. G.W., Z.Z., X.X., J.L., and H.M. contributed to Writing – review & editing. All authors reviewed the manuscript.

Competing interests

The authors declare no competing interests.

Reference

[1] F. Bray, M. Laversanne, H. Sung et al., Global cancer statistics 2022: GLOBOCAN estimates of incidence and mortality worldwide for 36 cancers in 185 countries. CA. Cancer J. Clin. 74, 229–263, (2024). https://doi.org/10.3322/caac.21834.

[2] R.L. Siegel, T.B. Kratzer, A.N. Giaquinto et al., Cancer statistics, 2025. CA. Cancer J. Clin. 75, 10–45, (2025). https://doi.org/10.3322/caac.21871.

[3] R.L. Siegel, A.N. Giaquinto and A. Jemal, Cancer statistics, 2024. CA. Cancer J. Clin. 74, 12–49, (2024). https://doi.org/10.3322/caac.21820.

[4] M. Lian, Y. Zhang, J. Huang et al., Lasiodin sensitizes hepatocellular carcinoma cancer to sorafenib via SNARE complex disruption. Phytomedicine. 149, 157603, (2025).

[5] M.E. Abdelsalam, K. Ahrar, R.A. Sheth et al., Interventional oncology: a primer for clinicians on the role of ablation and embolization for solid tumors. CA. Cancer J. Clin. 76, e70051, (2026). https://doi.org/10.3322/caac.70051.

[6] B. Sangro, M. Iñarrairaegui and J.I. Bilbao, Radioembolization for hepatocellular carcinoma. Journal of Hepatology. 56, 464–473, (2012). https://doi.org/10.1016/j.jhep.2011.07.012.

[7] J.-L. Raoul, E. Boucher, Y. Rolland et al., Treatment of hepatocellular carcinoma with intra-arterial injection of radionuclides. Nat Rev Gastroenterol Hepatol. 7, 41–49, (2010). https://doi.org/10.1038/nrgastro.2009.202.

[8] M.M. Welling, N. Duszenko, M.P. van Meerbeek et al., Microspheres as a carrier system for therapeutic embolization procedures: achievements and advances. J. Clin. Med. 12, 918, (2023). https://doi.org/10.3390/jcm12030918.

[9] R.J. Mumper, U.Y. Ryo and M. Jay, Neutron-activated holmium-166-poly (L-lactic acid) microspheres: a potential agent for the internal radiation therapy of hepatic tumors. J. Nucl. Med.: Off. Publ. Soc. Nucl. Med. 32, 2139–2143, (1991).

[10] J.F. Nijsen, A.D. van Het Schip, M.J. van Steenbergen et al., Influence of neutron irradiation on holmium acetylacetonate loaded poly(L-lactic acid) microspheres. Biomaterials. 23, 1831–1839, (2002). https://doi.org/10.1016/s0142-9612(01)00309-x.

[11] J.F. Nijsen, B.A. Zonnenberg, J.R. Woittiez et al., Holmium-166 poly lactic acid microspheres applicable for intra-arterial radionuclide therapy of hepatic malignancies: effects of preparation and neutron activation techniques. Eur. J. Nucl. Med. 26, 699–704, (1999). https://doi.org/10.1007/s002590050440.

[12] A.G. Arranja, W.E. Hennink, C. Chassagne et al., Preparation and characterization of inorganic radioactive holmium-166 microspheres for internal radionuclide therapy. Mater. Sci. Eng., C. 106, 110244, (2020). https://doi.org/10.1016/j.msec.2019.110244.

[13] S.W. Zielhuis, J.F.W. Nijsen, R. de Roos et al., Production of GMP-grade radioactive holmium loaded poly(L-lactic acid) microspheres for clinical application. Int J Pharm. 311, 69–74, (2006). https://doi.org/10.1016/j.ijpharm.2005.12.034.

[14] X. Xu, H. Chen, P. He et al., 3D Hollow Porous Radio - Granular Hydrogels for SPECT Imaging - Guided Cancer Intravascular Brachytherapy. Adv Funct Materials. 33, 2215110, (2023). https://doi.org/10.1002/adfm.202215110.

[15] X. Xu, H. Zhang, J. Ao et al., 3D hierarchical porous amidoxime fibers speed up uranium extraction from seawater. Energy & Environmental Science. 2019.

[16] X. Xu, H. Chen, Z. Zhao et al., Engineering radioactive microspheres for intra-arterial brachytherapy using radiation-induced graft polymerization. Adv. Funct. Mater. 33, 2306215, (2023). https://doi.org/10.1002/adfm.202306215.

[17] R.N. Darie-Niță, A. Irimia, F. Doroftei et al., Bioactive and physico-chemical assessment of innovative poly(lactic acid)-based biocomposites containing sage, coconut oil, and modified nanoclay. Int. J. Mol. Sci. 24, 3646, (2023).

https://doi.org/10.3390/ijms24043646.

[18] X. Xu, L. Xu, J. Ao et al., Ultrahigh and economical uranium extraction from seawater via interconnected open-pore architecture poly(amidoxime) fiber. J. Mater. Chem. A. 8, 22032–22044, (2020). https://doi.org/10.1039/D0TA07180C.

[19] J.F. Nijsen, A.D. Schip, W. Hennink et al., Advances in nuclear oncology: microspheres for internal radionuclide therapy of liver tumours. Curr. Med. Chem. 9, 73–82, (2002). https://doi.org/10.2174/0929867023371454.

[20] A. Vogel, S.L. Chan, L.A. Dawson et al., Hepatocellular carcinoma: ESMO clinical practice guideline for diagnosis, treatment and follow-up. Ann. Oncol. 36, 491–506, (2025). https://doi.org/10.1016/j.annonc.2025.02.006.

[21] C. Kratochwil, W.P. Fendler, M. Eiber et al., EANM procedure guidelines for radionuclide therapy with 177Lu-labelled PSMA-ligands (177Lu-PSMA-RLT). Eur. J. Nucl. Med. Mol. Imaging. 46, 2536–2544, (2019). https://doi.org/10.1007/s00259-019-04485-3.

[22] H. Cai HW (Cai, F. Pang FW (Pang, W. Zhang WJ (Zhang et al., Preparation of 131I-collagen-chitosan microspheres for interventional radionuclide therapy. J. Nucl. Med. (2016).

[23] J.J. Zaknun, L. Bodei, J. Mueller-Brand et al., The joint IAEA, EANM, and SNMMI practical guidance on peptide receptor radionuclide therapy (PRRNT) in neuroendocrine tumours. Eur. J. Nucl. Med. Mol. Imaging. 40, 800–816, (2013). https://doi.org/10.1007/s00259-012-2330-6.

[24] X. Jiang, L. Chen and X. Xu, Advancements in the investigation of radioactive microspheres for brachytherapy. Front. Bioeng. Biotechnol. 13, 1621418, (2025). https://doi.org/10.3389/fbioe.2025.1621418.

[25] Z. Zhao, Y. Chen, H. Liu et al., Amidoxime-based radio-microspheres for internal irradiation combined with a checkpoint-blocking nanobody boost antitumor immunity. Nano Today. 57, 102383, (2024). https://doi.org/10.1016/j.nantod.2024.102383.

[26] L. Xiao, Y. Li, R. Geng et al., Polymer composite microspheres loading 177Lu radionuclide for interventional radioembolization therapy and real-time SPECT imaging of hepatic cancer. Biomater. Res. 27, 110, (2023). https://doi.org/10.1186/s40824-023-00455-x.